



The SoilExp software: An open-source Graphical User Interface (GUI) for post-processing spatial and temporal soil surveys

G. Boudoire, M. Liuzzo, S. Cappuzzo, G. Giuffrida, P. Cosenza, A. Derrien,
E.E. Falcone

► To cite this version:

G. Boudoire, M. Liuzzo, S. Cappuzzo, G. Giuffrida, P. Cosenza, et al.. The SoilExp software: An open-source Graphical User Interface (GUI) for post-processing spatial and temporal soil surveys. Computers & Geosciences, 2020, 142, pp.104553. 10.1016/j.cageo.2020.104553 . hal-02901361

HAL Id: hal-02901361

<https://uca.hal.science/hal-02901361>

Submitted on 4 Sep 2020

HAL is a multi-disciplinary open access archive for the deposit and dissemination of scientific research documents, whether they are published or not. The documents may come from teaching and research institutions in France or abroad, or from public or private research centers.

L'archive ouverte pluridisciplinaire **HAL**, est destinée au dépôt et à la diffusion de documents scientifiques de niveau recherche, publiés ou non, émanant des établissements d'enseignement et de recherche français ou étrangers, des laboratoires publics ou privés.

The SoilExp software: an open-source Graphical User Interface (GUI) for post-processing spatial and temporal soil surveys

G. BOUDOIRE^{1,2*}, M. LIUZZO¹, S. CAPPUZZO¹, G. GIUFFRIDA¹, P. COSENZA¹,
A. DERRIEN³, E.E. FALCONE¹

¹Istituto Nazionale di Geofisica e Vulcanologia, Sezione di Palermo, Via Ugo La Malfa
153, 90146 Palermo, Italy

²Université Clermont Auvergne, CNRS, IRD, OPGC, Laboratoire Magmas et Volcans,
6 avenue Blaise Pascal, 63178 Aubière, France

³Observatoire Volcanologique du Piton de la Fournaise (OVPF), Institut de Physique
du Globe de Paris (IPGP), Sorbonne Paris-Cité, UMR 7154 CNRS, Université Paris
Diderot, Bourg Murat, France

* Corresponding author. Present address: Laboratoire Magmas et Volcans – 6 avenue
Blaise Pascal – 63170 Aubière (France). Telephone: +33 07 85 22 19 11. E-mail:
guillaume.boudoire@uca.fr

G. Boudoire has developed the SoilExp software, and performed field and laboratory tests. M. Liuzzo has conceived and designed the MEGA instrument and performed field and laboratory tests. S. Cappuzzo has conceived and designed the MEGA instrument. G. Giuffrida has performed field and laboratory tests. P. Cosenza has contributed to the design of MEGA instrument. A. Derrien has performed field tests and E.E. Falcone contributed to the writing of the manuscript.

Abstract

Preliminary interpretation of geological processes during field measurement campaigns require fast data analysis to adapt ongoing target strategies. It is the case of soil investigations where coupling geochemical and geophysical records favor a better understanding of subsurface processes. This task requires (i) statistical analysis ~~is needed~~ to identify areas of interest during spatial surveys and (ii) signal processing ~~is required~~ to analyze temporal series.

Here we present SoilExp, an open-source Python-based Graphical User Interface (GUI) that permits to process spatial and temporal surveys of soil gases (e.g. soil CO₂ flux) combined with common physical parameters (e.g. self-potential, temperature) that are synchronously recorded on the field. SoilExp mixes innovative algorithms with the more common tools used for the analysis of both spatial surveys or temporal series. It offers the possibility to display distribution plots, maps, comparative plots, spectra and spectrograms, as well as data statistical analysis, in order to deal efficiently with datasets acquired on the field. Field measurements performed at Stromboli (Italy) supports that such software solution facilitates a quick visualization of the data output and is a powerful tool on the geochemical and geophysical analysis.

Keywords

Geo-spatial survey, time series, soil CO₂ degassing, self-potential, Python

1. Introduction

Identifying hidden geologic structures and studying gas and hydrothermal fluid circulation within the ground is of first interest in many disciplines as agriculture (Kucera & Kirkham, 1971), mineral resources (Hinkle & Dilbert, 1984; Lovell *et al.*,

1983), geothermy (Chiodini *et al.*, 2001, 2005), geological storage (Sandig *et al.*, 2014) and natural hazards (Allard *et al.*, 1991; Finizola *et al.*, 2002; Hernandez *et al.*, 2001; Irwin & Barnes, 1980). Coupling geochemical and geophysical records has demonstrated a real complementarity to characterize soil heterogeneities and related fluid circulations (Aubert *et al.*, 1984; Boudoire *et al.*, 2018; Elskens *et al.*, 1964; Finizola *et al.*, 2003; Gaudin *et al.*, 2015; Giammanco *et al.*, 1997). In particular, diffusive CO₂ degassing (CO₂), self-potential (SP) and temperature (T) measurements are among the most common methods used by the scientific and industrial community to perform both spatial surveys or temporal records for monitoring purposes (Boudoire *et al.*, 2018; Byrdina *et al.*, 2012; Finizola *et al.*, 2003; Gresse *et al.*, 2016; Pearson *et al.*, 2008).

These measurements often require (i) the use of self-alone instruments and (ii) a preliminary data treatment to be used reliably. For instance, (i) measurements of diffusive CO₂ degassing (CO₂) may require the use of a stainless steel probe (active method) or an accumulation chamber (passive method) connected to infrared spectrometers, self-potential may require the use of non-polarizable Cu/CuSO₄ electrodes coupled with a high impedance voltmeter and temperature (T) measurements may be performed with K-type thermal probes and a digital thermometer or with a pyrometer (Finizola *et al.*, 2010). Additionally (ii), spatial surveys often need a quick first idea of results during the daily performed acquisitions in order to identify the main areas of interests and eventually adapt or correct the ongoing fieldwork strategy (Chatterjee *et al.*, 2019). Meanwhile, temporal series are often subjected to an environmental influence that needs to be corrected before an accurate use of the signals as regression, moving average or cut-band filter for the most common ones (Boudoire *et al.*, 2017a; Liuzzo *et al.*, 2013; Padron *et al.*, 2008; Viveiros *et al.*, 2008). Many industrial software packages or homemade codes are able to deal efficiently with this

kind of data but often required to be used additionally to cover the whole range of expected common data treatment tools (with various file formatting). It is often time consuming and limit a fast and efficient evaluation of the datasets.

Here we present a new user-friendly Python-based GUI (Graphical User Interface) software: Soil Exploration (SoilExp). SoilExp is able to analyze both spatial and temporal datasets obtained on the field and respecting some file formatting rules. The final aim of SoilExp is to provide to the geologic-environmental researchers community both innovative and classical tools for a first data processing: (i) data correction (linear regression, moving average, cut-band filter), (ii) data analysis (statistical analysis, populations identification), (iii) data comparison (correlations, cross-correlations) and, (iv) graphical representation (distribution plots, comparative plots, spectra, spectrograms, maps). To illustrate the potentiality of SoilExp to sustain field surveys and to address scientific issues, both soil CO₂ flux and self-potential measurements were performed at Stromboli (Italy). Results are presented in a final section and discussed with respect to those obtained from previous field surveys.

2. Overview on the SoilExp software

The SoilExp 1.0 software distribution is written in Python 2.7 (Fig. 1). The Graphical User Interface (GUI) is based on the Tkinter library. It requires the following libraries: Pandas, Numpy, SciPy, Matplotlib, Scikit-Learn, PySerial is required. Thus, as processed during SoilExp 1.0 development, we recommend to the user to install the Anaconda distribution on their machines in order to benefit of the Spyder open source cross-platform integrated development environment (IDE) with scientific libraries. Full details are provided in the user guide. Information related to the installation of the software distribution (SoilExp 1.0), to its step-by-step use and to potential script modifications are reported in the associated user manual.

Indeed, in this study, we focus on the main functionalities provided by the SoilExp 1.0 distribution. These main functionalities are exposed through three independent scripts described in the following parts (Fig. 2). The first script is dedicated to save/reset field data from the MEGA (Multisensors Electrical and Gas Analyzer) instrument and calibrate its sensors using an USB-Serial connection (so-called “Serial” option in the following parts) (Fig. 3a). The second script is dedicated to the analysis of spatial surveys (so-called “Space” option in the following parts) (Fig. 3b). The third script is dedicated to time series processing (so-called “Time” option in the following parts) (Fig. 3c).

The “Serial” option is dedicated for applications based on the use of the MEGA instrument that has been entirely conceived and designed at the INGV of Palermo by two of the current authors (Liuzzo & Cappuzzo). The MEGA instrument is not the focus of this paper and will be better presented to the community in future specific contributions. The other two options are composed of four panels (Fig. 3): (i) the first one (e.g. ‘1. File Treatment’) is used to treat raw data files and create intermediate formatted files; (ii) the second one (e.g. ‘2. Data Processing’) is used to select a parameter of interest from an intermediate formatted file, modify its corresponding series (correction, filtering, average) and, display resulted plots (for the “Time” option); (iii) the third one (e.g. ‘3. Data Analysis’) is dedicated to show the results of the data analysis as correlations, cross-correlations, statistics, populations identification and plots (for the “Space” option); (iv) the last one (e.g. ‘4. Save’) is used to save final processed datasets and related information (as populations) in .csv files.

3. Main functionalities

3.1. Initialization

The initialization step (first panel of the “Time” and “Space” options) aims at converting raw data files to intermediate files that may be manipulated in the other panels (Fig. 3b, c). Raw data files are “.csv” files downloaded from the MEGA instrument or created by the user in a compatible format to be correctly processed (see the user manual).

In the “Space” and “Time” options (Fig. 3b, c) the user can choose either the instrumental calibration by default or new calibration parameters to recalculate data series. Data reduction then performed in order to identify internal errors (typographical errors) or unreliable measurements, i.e. out of the range of values defined for the battery voltage, the pump flux and the horizontal dilution of precision (HDOP) of the global positioning system (GPS). These limit values used to define outliers are set by default but may be changed by the user directly in the GUI. Rows containing bad values are either linearly interpolated with the “Time” option in order to correctly apply further time series analysis (in this case interpolated rows are kept in memory in order to be removed in final .csv files) or left as empty rows with the “Space” option. Additionally, as soil CO₂ measurements may be acquired with the accumulation chamber method in the “Space” option, an additional filter is applied on the r-squared value of computed soil CO₂ flux. In this case, values of soil CO₂ flux out of the r-squared range will be considered as outliers values and thus set at 0 gm⁻²d⁻¹ (no flux). In the case where soil CO₂ flux has to be calculated from the dynamic concentration method, the software integrates the possibility in both options to convert the CO₂ %molar contents in flux (Camarda *et al.*, 2006; Gurrieri and Valenza, 1988; Liuzzo *et al.*, 2015). The conversion is made by the use of the equation of Camarda *et al.* (2006) that takes into account the soil permeability value defined by the user.

Once the raw data file is cleaned, the last step will generate intermediate files that are of first interests to keep processing the data thanks to the other panels of the

GUI. The definition of the time-lag period (in seconds) is here fundamental. We define the time-lag as the period in seconds separating two independent series of measurements (i.e. the period during which the used instrument will be in stand-by). With the “Time” option, a new intermediate file will be created each time that two consecutive rows are separated by a duration greater than the time-lag. With the “Space” option, an unique intermediate file will be created with the median values of each independent series (the median value being here considered as representative of the acquisition to avoid the effect of potential spikes on the average). The time-lag must not be confused with the sampling rate that is necessary shorter and defines the period (in seconds) between two measurements within the same series. The sampling rate is used to correctly adapt the scale and the legend of plots (spectra, spectrogram) by converting a range of measurements (number of records) into a time range (number of seconds).

3.2. The “Space” option: dealing with spatial surveys

The “Space” option aims to propose innovative and classical tools to deal with spatial surveys, i.e. with datasets where each point of measurements is defined by distinct geographical coordinates (Fig. 3b).

3.2.1. Correlations and preliminary data correction

The “Space” option allows coefficients of linear correlations to be identified (slope, offset, r-squared) between the parameter of interest (e.g. CO₂) and other records (e.g. temperature, pressure, wind speed) obtained by the user (Fig. 3b). In particular, these coefficients are often useful during soil surveys, where records can be affected by external parameters. For instance, soil CO₂ flux may be slightly dependent on pressure

(Barde-Cabusson *et al.*, 2009; Liuzzo *et al.*, 2013; Viveiros *et al.*, 2008). The equation used for the linear regression is the following:

$$Signal_{Clr}(x,y) = Signal_{Raw}(x,y) - (a \times (Param_{Raw}(x,y) - Param_{Avg}))$$

where $Signal_{Clr}(x,y)$ is the value of the parameter of interest at the geographical position (x,y) after the correction by linear regression, $Signal_{Raw}(x,y)$ is the value before the correction, a is the slope of the linear correlation, $Param_{Raw}(x,y)$ is the parameter used to performed the regression at the geographical position (x,y) and, $Param_{Avg}$ is the average of this parameter for the whole dataset in order to correct the offset linked to the correction. After the correction, coefficients of linear correlations are reprocessed and automatically updated in order to verify the efficiency of the correction and identify potential needs of further steps of correction.

3.2.2. Statistical analysis

In order to better constrain the data distribution of the parameter of interest, the “Space” option allows the user to display also a probability histogram together with the best fit line of the potential normal distribution (see Supplementary Material). The normality of the data series is tested via the Anderson-Darling normality test (SciPy library; Anderson and Darling, 1952; Stephens, 1974, 1976). In our case, i.e. making the assumption that both mean and variance are initially unknown, the Anderson-Darling normality test rejects the hypothesis of normality with a 95% significance level if A^2 (the squared of the test statistic A) exceeds 0.752 for data series owning more than 8 samples (D’Agostino, 1986).

Together with the Anderson-Darling normality test, the “Space” option gives the opportunity to calculate some classical statistical values: mean, standard deviation,

median, minimum, maximum, kurtosis, skewness (Fig. 3b). Here we focus on the last two indicators less common for non-regular users of statistical tools. The kurtosis is a measure of the tailedness of the probability distribution of a random variable, i.e. describing the shape of the probability distribution (Zwillinger and Kokoska, 2000). Using the Fisher's definition, normally distributed data should provide a result of 0. Skewness is the measure of the asymmetry of the probability distribution of a random variable with respect to its mean. The skewness, which could be either positive or negative, should be about 0 for normally distributed data (Zwillinger and Kokoska, 2000).

If the indicators described above (skewness, kurtosis, Anderson-Darling normality test) do not argue in favor of a normal distribution, it may be due to the presence of more than one population in the data series. Indeed, during spatial survey, one subject of major interest is often to discriminate the different populations that contribute to the data series. This is crucial in order to recognize the existence of distinct sources as, for example, biogenic or magmatic ones for soil CO₂ flux in volcanic context (Boudoire *et al.*, 2017b; Liuzzo *et al.*, 2015; Viveiros *et al.*, 2008). In order to address this specific issue, we have developed a new algorithm in SoilExp able to combine the two statistical methods more used in environmental scientific research, which can distinguish various populations from log-normally distributed data (Fig. 4a, b). The first is the graphical method based on probability plots known as Sinclair method (Chiodini *et al.*, 1998; Giammanco *et al.*, 2010; Sinclair, 1974); the second is the maximum-likelihood numerical method based on the use of Gaussian Mixture Model (GMM) implementing an expectation-maximization (EM) algorithm (Benaglia *et al.*, 2009; Boudoire *et al.*, 2018; Elio *et al.*, 2016). The Sinclair method provides an user-friendly view of the populations and mixed values, however, it has two main shortcomings. One is related to the low accuracy for datasets counting less than 100 values (Sinclair, 1974).

The second limitation is related to the difficulty to precisely estimate the confidence intervals. These problems are solved using the maximum-likelihood (ML) method that fits finite mixtures of normal distributions: we have implemented a Scikit-Learn-based algorithm that simulates such fitting with 1 to 10 populations with 1000 iterations for each simulation. The best simulation is then selected based on the value of the Bayesian Information Criterion (BIC) developed for model selection among finite set of simulations (Ghosh *et al.*, 2006) and displayed on the GUI (Fig. 3b) . Finally, for each value of the data serie, the algorithm predicts the probability that the value belongs to one of the defined populations. In our case, we have considered that if one value shows a probability to be defined by a single population greater than 95% thus it will be considered as part of this population. If not, this value is considered as an intermediate value (or mixed value) between the two neighboring populations. At the end, the algorithm allows the user to automatically see the result of this ML-based partitioning of the values on probability plots (Fig. 4a, b). Furthermore, the users can simulate different partitioning by modifying the number of inferred populations directly on the GUI (Fig. 3b), if the first step of differentiation is not satisfying.

3.2.3. Mapping

After having performed data correction and statistical analysis, it is possible to obtain a first idea of the two-dimensions (2D) distribution of the data (Fig. 4c, d). Our aim is not to develop complex interpolating algorithms for which many software are already built. Here we propose a simple graphical representation of the data through two distinct maps. The first one uses a simple color gradient to show the 2D evolution of the values. The second one is more innovative (presented on Fig. 4 for SP and CO₂ data obtained at Stromboli), meaning that the map-builder takes into consideration the results of the population analysis described above, generating and displaying a repartition of the

values between the different populations (and related mixing values). If an internet connection and an API key are available (<https://developers.google.com/maps/documentation/javascript/get-api-key>), a background satellite map will be automatically downloaded and georeferenced from the Google Maps Platform. If not, the background will remain neutral. However, the upper left box (Fig. 4c, d) highlights the coordinates of the corners to facilitate the extraction of an adequate background map from other sources.

3.3. The “Time” option: processing time series

The “Time” option aims to propose classical tools to deal with time series, i.e. with datasets where the measurements have specific frequency (here defined as the sampling rate) (Fig. 3c).

3.3.1. Correlations and cross-correlations

“Time” option allows to identify coefficients of linear correlations (slope, offset, r-squared) between the parameter of interest and other records, where the control panel (Fig. 3c) is similar to the one in "Space" option. Sometimes some signals may have a time delay between them, which can be attributed either to an instrumental lag or to an effect caused by a natural phenomenon. To take into account these effects, we have implemented a SciPy-based algorithm to calculate the cross-correlations between each parameters. The algorithm couples complex-valued functions with conjugates and Fast Fourier Transform (FFT) to numerically determine both lags and r-squared values between time series. Best results are shown in the table of the “Time” option GUI (Fig. 3c).

3.3.2. Signal processing

The “Time” option gives the possibility to the user to apply three of the most common signal processing tools used in the geo-scientific community: (i) linear regression, (ii) moving average and, (iii) cut band filter.

The linear regression method is the same than in the “Space” option and only require to select the parameter used for the regression and to compute the corresponding coefficients. This method is used to remove short-term environmental influence on geochemical and geophysical signals (Boudoire *et al.*, 2017a; Liuzzo *et al.*, 2013).

The moving average method is a type of finite impulse response filter used to smooth out short-term signal variations. This method performs an average on a defined subset of the data series, then shifts forward to repeat the calculations, excluding the first value of the previous subset and including the next one. Using the convolution operator of the Numpy library, we have implemented a simple moving average method, i.e. giving the same weight to each value a_j :

$$movav(a_i) = \left(\frac{1}{k}\right) \times \sum_{j=i-k/2}^{i+k/2} a_j \text{ for } i \in \left] \frac{k}{2}, \frac{n-k}{2} \right[$$

where i is the position of the value a_i in the data series on which the moving average is applied, n the length of the data series and k the size of the subset. To deal with border effects (i.e. when the number of available values to perform the moving average is lower than the size of the defined subset), we have adapted the convolution to the number of available values:

$$movav(a_i) = \left(\frac{1}{i}\right) \times \sum_{j=0}^i a_j \text{ for } i \in \left[0, \frac{k}{2} \right]$$

$$306 \quad movav(a_i) = \left(\frac{1}{n-i}\right) \times \sum_{j=i}^n a_j \text{ for } i \in \left[\frac{n-k}{2}, n\right]$$

307

308 To enhance the reliability of the calculations linked to correlations and cross-
 309 correlations, the moving average method is applied to all data series when computed.

310 Finally, to treat long-term signal variations, we have used the Fast Fourier
 311 Transform (FFT) package of the SciPy library to develop a cut (or block) band filter.
 312 This filter removes from the signal spectra (cf. ‘*fft*’) the frequencies belonging to an
 313 interval defined by the user before making the inverse operation to rebuild the signal
 314 (cf. ‘*ifft*’).

315

316 **3.3.3. Graphical representation**

317 When pressing the plot-related buttons of the “Time” option, the user automatically
 318 applies the correction and filtering methods that has been defined previously (Fig. 2).

319 Consequently, the user may decide to perform several combination between the
 320 signals which is intended to compare:

- 321 (i) Compare the raw signal with the new corrected and filtered signal, and
 322 eventually reinitialize the signal to apply a distinct protocol (Fig. 5a). Based
 323 on the same statistical algorithm used with the “Space” option to
 324 characterize populations, we have implemented an option allowing the user
 325 to directly show on the plot the values belonging to the “highest” population
 326 (often considered as representative of anomalous values with respect to the
 327 background; Boudoire *et al.*, 2017a; Liuzzo *et al.*, 2013, Liuzzo *et al.*, 2015);
- 328 (ii) Compare the treated signal with another signal of interest (Fig. 5b). This
 329 plot may be particularly useful to investigate well correlated or cross-
 330 correlated signals;

- (iii) See the FFT spectrum on which are displayed the three greatest frequencies (Fig. 5c). Thanks to the labels indicating the corresponding number of measurements, the user may define the frequency interval on which applying the cut-band filter;
- (iv) See the corresponding spectrogram that is a different visual representation of the FFT spectrum, extensively used in geophysical signal processing (Fig. 5d). It is particularly useful to detect periodic components and signal perturbations that may affect all frequencies. Here we use the '*specgram*' function of the Matplotlib library with a linear detrend and a magnitude mode of 256 NFFT of default (Nonequispaced Fast Fourier Transform: the number of points in each processed block) and a 128 noverlap (the number of points of overlap between processed blocks). The user is free to modify these parameters directly in the Python 2.7 script (see user manual).

The signal analysis depends on the sampling rate, therefore we cannot use an unique legend for spectrum and spectrogram axes. Consequently, we have adapted the algorithms to show both the results of the raw signal analysis (in term of number of measurements) and their meaning using more classical units. For the last one, we have coupled the number of measurements and the sampling rate to have a real temporal scale (i) in seconds (between parenthesis) on the spectrum and (ii) in hertz on the spectrogram.

3.4. Saving and exporting results

The SoilExp software gives the opportunity to save every graphical object with different extensions (.png, .eps ...), which can be easily further modified later.

Additionally both "Space" and "Time" GUI options have dedicated buttons to save .csv files. In the "Space" option, the final .csv file is similar to the intermediate

file but takes into account the results of the linear regressions that could be applied to correct the dataset. Additionally, it is possible to save a .csv file recording the data repartition between the defined populations and mixing groups. Both files aim to be eventually further processed through software dedicated to complementary and more specific tools as e.g. data interpolation, kriging, sequential Gaussian simulation (SGS). In the “Time” option, the final .csv file is also similar to the intermediate file but (i) has one supplemental column for the corrected and filtered data series and (ii) shows empty rows for missing values, which have been interpolated for the needs of signal processing. Such final file may be then processed through other complementary software for measurements of volcanic gas in plume or other environmental applications in atmospheric measurements (Fig. 1e, f).

4. SoilExp application: an example at Stromboli (Italy)

In volcanic environment, two of the main goals of soil surveys are (i) the identification of volcano-tectonic structures (Giammanco et al., 1997; Finizola et al., 2002, 2010) and (ii) the characterization of hydrothermal fluid circulation (Revil et al., 2011; ; Boudoire et al., 2018). Once, because these low permeable structures may favor the ascent of magmatic fluids leading to fissural eruptions (Boudoire et al., 2017b). Moreover, such structural interfaces may raise important issues concerning soil stability and thus landslide outbreak (Neri et al., 2004). To test the ability of SoilExp to deal with such goals, we have performed a spatial soil survey at Stromboli (Sicily, Italy) by the mean of the MEGA instrumental kit (Fig. 1). Three transects were performed with a 20 m-spacing for a total of 45 measurements of soil CO₂ flux and self-potential (dataset available with our distribution as “intermediate” test file). Here, we focused on the first transect (14 measurements), the one on the northern flank of the volcano which is the closest to populated areas (Fig. 1c).

383 Data analysis performed with the “Space” option of SoilExp reveals (i) the
 384 absence of correlation between soil CO₂ ‘dynamic’ concentration (‘CO2_10’) and the
 385 environmental parameter (pressure ‘P_atm’, temperature ‘T_atm’, humidity ‘Rh’)
 386 during the transect and (ii) an important correlation ($R^2 = 0.79$) between soil CO₂
 387 ‘dynamic’ concentration (‘CO2_10’) and self-potential measurements (‘SP’).
 388 Consequently, no correction from the environmental influence was applied (Viveiros
 389 et al., 2008) and we focus on both soil CO₂ flux and self-potential measurements in the
 390 following parts. The analysis performed by SoilExp shows that soil CO₂ ‘dynamic’
 391 concentration (‘CO2_10’) varies from 0.07 to 0.95 %. Self-potential (‘SP’) varies from
 392 -155 to +77 mV. The Anderson-Darling normally test gives A² equal to 14.3 and 3.3
 393 for ‘CO2_10’ and ‘SP’, respectively. These values are well above 0.752, and testify
 394 that both datasets do not present a normal distribution (at 95% of significance level). It
 395 means that these datasets are better explained by the presence of two or more
 396 populations. Actually, the new statistical algorithm developed in SoilExp highlights the
 397 presence of two populations of values for both parameters (Fig. 4a, b). Soil CO₂
 398 ‘dynamic’ concentration shows the presence of two populations: one with high values
 399 (>0.20 % for 7.1% of the dataset; Fig. 4a) and the other with low values (<0.20 % for
 400 92.9% of the dataset). We applied the equation of Camarda et al. (2006) to convert soil
 401 CO₂ ‘dynamic’ concentration in soil CO₂ flux for a range of soil permeability between
 402 15 and 50, i.e. the most common values for volcanic soils (Camarda et al., 2006). The
 403 calculated upper limit of the population of low soil CO₂ flux does not exceed 42 gm⁻²d⁻¹
 404 ¹. This value is in accordance with the definition of a “background” population
 405 characterized by low soil CO₂ flux and generally ascribed to the biological soil activity
 406 (Liuzzo et al., 2015; Boudoire et al., 2017b). Conversely, the population of higher soil
 407 CO₂ flux (up to 233 gm⁻²d⁻¹) is consistent with a magmatic-hydrothermal origin of the
 408 released fluids (Giammanco et al., 1997; Liuzzo et al., 2015). Self-potential shows also

the presence of one population of high values (from -9 up to +77 mV for 14.3% of the dataset; Fig. 4b) whereas most of the dataset is defined by a population of more negative values (from -169 up to -100 mV for 85.7% of the dataset).

Interestingly, the map-building of the soil CO₂ ‘dynamic’ concentration (Fig. 4c) and self-potential (Fig. 4d), based on this population analysis, shows that the population of high soil CO₂ ‘dynamic’ concentration spatially correlates with the high self-potential measurements. This positive correlation between the two parameters is consistent with an upward migration of hydrothermal fluids in a restricted part of the transect (<40 m-wide) as documented for other volcanic systems (Barde-Cabusson et al., 2009; Bennati et al., 2011). Actually, this restricted part of the transect is cut by the Nel Cannestrà eruptive fissure that is known representing a low permeability structure, in relation with N41° inferred regional faults, (Finizola et al., 2002, 2010; Carapezza et al., 2009). The identification and characterization of such structure that favors the ascent of magmatic fluids raise important civil protection issues (Boudoire et al., 2017b). Current monitoring is performed in this area by the Istituto Nazionale di Geofisica e Vulcanologia (INGV) (Carapezza et al., 2009).

5. Conclusion

In this work we presented an open-source Graphical User Interface (GUI) software, SoilExp, which is written in Python language and is able to provide statistical and spectrum analysis as well as several options on filtering and correcting analysis on records acquired during spatial/temporal surveys. The software is based on two main options. Firstly, the “Space” option, aims to display the main statistical indicators used to study spatial surveys, to test the normality of data series, to identify and define the populations constituting the dataset through an innovative algorithm, and to show results on satellite maps. The second one, the “Time” option, aims to process time series

through classical tools used in signal processing (linear regression, moving average, cut-band filter, cross-correlations) and in signal representations (scatter plots, spectra, spectrogram). Beyond facilitating the fast outcome from field surveys by offering filtering tools, graphical results and statistical analyses, SoilExp gives to the users the possibility to integrate all the results in a unique tool of elaboration, improving the research potential of the scientific community dealing with spatial and temporal soil surveys.

Acknowledgments

S. Gurrieri is acknowledged for constructive discussions and advices on the script. P. Boudoire, A. Finizola and T. Ricci are acknowledged for providing technical support crucial for instrumental tests. People proposing or commenting open source Python codes and solutions on forums are gratefully acknowledged. We thank the Associate Editor and Jean Vandemeulebrouck for their suggestions that greatly improved the clarity and quality of the paper. This work has been funded by the Fondo Sociale Europeo (PO FSE 2014-2020) in the frame of the project “Metodi di controllo geochimico e geofisico dei fenomeni naturali sul campo ed in laboratorio”. We also acknowledge the French government IDEX-ISITE initiative 16-IDEX-0001 (CAP 20-25).

Computer code availability

The SoilExp software including full scripts, user manual and example files may be freely downloaded from <https://github.com/FreeMindsObservatory/SoilExp> (main developer: Dr. Guillaume Boudoire; corresponding author). The first distribution started to be developed in 2017 (SoilExp 1.0 based on Python 2.7; 16.6 Mo), made available for MacOSX and Windows platforms. It may be modified by any contributor

according his needs thanks to a Creative Commons Attribution-NonCommercial-ShareAlike 4.0 International License (CC BY-NC-SA 4.0) (<https://creativecommons.org/licenses/by-nc-sa/4.0/>). The software requires the installation of the Anaconda distribution to use the Spyder open source cross-platform integrated development environment (IDE) integrated all required scientific libraries. Please contact the corresponding author for any support regarding the SoilExp software.

References

- Allard, P., Carbonnelle, J., Dajlevic, D., Le Bronec, J., Morel, P., Robe, M.C., Maurenas, J.M., Faivre-Pierret, R., Martin, D., Sabroux, J.C., Zettwoog, P., 1991. Eruptive and diffuse emissions of CO₂ from Mount Etna. *Nature* 351(6325), 387-391.
- Anderson, T.W., Darling, D. A., 1952. Asymptotic theory of certain "goodness-of-fit" criteria based on stochastic processes. *Annals of Mathematical Statistics* 23, 193–212, doi:10.1214/aoms/1177729437.
- Aubert, M., Camus, G., Fournier, C. 1984. Resistivity and magnetic surveys in groundwater prospecting in volcanic areas—case history maar of Beaunit, Puy de Dome, France. *Geophysical prospecting* 32(4), 554-563.
- Barde-Cabusson, S., Finizola, A., Revil, A., Ricci, T., Piscitelli, S., Rizzo, E., Angeletti, B., Balasco, M., Bennati, L., Byrdina, S., Carzaniga, N., Crespy, A., Di Gangi, F., Morin, J., Perrone, A., Rossi, M., Roulleau, E., Suski, B., Villeneuve, N., 2009. New geological insights and structural control on fluid circulation in La Fossa cone (Vulcano, Aeolian Islands, Italy). *J. Volcanol. Geotherm. Res.* 185, 231–245, doi: 10.1016/j.jvolgeores.2009.06.002.

486

487 Benaglia, T., Chauveau, D., Hunter, D., Young, D., 2009. mixtools : An R package for
488 analyzing finite mixture models. *Journal of Statistical Software* 32(6), 1-29.

489

490 Bennati, L., Finizola, A., Walker, J.A., Lopez, D.L., Higuera-Diaz, I.C., Schütze, C.,
491 Barahona, F., Cartagena, R., Conde, V., Funes, R., 2011. Fluid circulation in a complex
492 volcano-tectonic setting, inferred from self-potential and soil CO₂ flux surveys: the
493 Santa María–Cerro Quemado–Zunil volcanoes and Xela caldera (Northwestern
494 Guatemala). *J. Volcanol. Geotherm. Res.* 199 (3–4), 216–229.
495 <http://dx.doi.org/10.1016/j.jvolgeores.2010.11.008>.

496

497 Boudoire, G., Di Muro, A., Liuzzo, M., Ferrazzini, V., Peltier, A., Gurrieri, S., Michon,
498 L., Giudice, G., Kowalski, P., Boissier, P., 2017a. New perspectives on volcano
499 monitoring in a tropical environment: continuous measurements of soil CO₂ flux at
500 Piton de la Fournaise (La Réunion Island, France). *Geophysical Research Letters*
501 44(16), 8244-8253.

502

503 Boudoire, G., Finizola, A., Di Muro, A., Peltier, A., Liuzzo, M., Grassa, F., Delcher,
504 E., Brunet, C., Boissier, P., Chaput, M., Ferrazzini, V., Gurrieri, S., 2018. Small-scale
505 spatial variability of soil CO₂ flux: Implication for monitoring strategy. *Journal of*
506 *Volcanology and Geothermal Research* 366, 13-26.

507

508 Boudoire, G., Liuzzo, M., Di Muro, A., Ferrazzini, V., Michon, L., Grassa, F., Derrien,
509 A., Villeneuve, N., Bourdeu, A., Brunet, C., Giudice, G., Gurrieri, S., 2017b.
510 Investigating the deepest part of a volcano plumbing system: evidence for an active

511 magma path below the western flank of Piton de la Fournaise (La Réunion Island).
 512 Journal of Volcanology and Geothermal Research 341, 193-207.
 513
 514 Byrdina, S., Rücker, C., Zimmer, M., Friedel, S., Serfling, U., 2012. Self potential
 515 signals preceding variations of fumarole activity at Merapi volcano, Central Java.
 516 Journal of Volcanology and Geothermal Research 215, 40-47.
 517
 518 Camarda, M., Gurrieri, S., Valenza, M., 2006. In situ permeability measurements based
 519 on a radial gas advection model : Relationships between soil permeability and diffuse
 520 CO₂ degassing in volcanic areas. Pure and applied geophysics 163(4), 897-914.
 521
 522 Carapezza, M.L., Ricci, T., Ranaldi, M., Tarchini, L., 2009. Active degassing structures
 523 of Stromboli and variations in diffuse CO₂ output related to the volcanic activity.
 524 Journal of Volcanology and Geothermal Research 182(3-4), 231-245.
 525
 526 Chatterjee, S., Deering, C.D., Waite, G.P., Prandi, C., Lin, P., 2019. An adaptive
 527 sampling strategy developed for studies of diffuse volcanic soil gas emissions. Journal
 528 of Volcanology and Geothermal Research.
 529
 530 Chiodini, G., Cioni, R., Guidi, M., Raco, B., Marini, L., 1998. Soil CO₂ flux
 531 measurements in volcanic and geothermal areas. Applied Geochemistry 13(5), 543-
 532 552.
 533
 534 Chiodini, G., Frondini, F., Cardellini, C., Granieri, D., Marini, L., Ventura, G., 2001.
 535 CO₂ degassing and energy release at Solfatara volcano, Campi Flegrei, Italy. Journal of
 536 Geophysical Research : Solid Earth 106(B8), 16213-16221.

537

538 Chiodini, G., Granieri, D., Avino, R., Caliro, S., Costa, A., Werner, C., 2005. Carbon
539 dioxide diffuse degassing and estimation of heat release from volcanic and
540 hydrothermal systems. *Journal of Geophysical Research : Solid Earth* 110(B8).

541

542 D'Agostino, R.B., 1986. Tests for the Normal Distribution. In *Goodness-of-Fit*
543 *Techniques*. New York, Marcel Dekker, ISBN 0-8247-7487-6.

544

545 Elio, J., Ortega, M.F., Nisi, B., Mazadiego, L.F., Vaselli, O., Caballero, J., Chacon, E.,
546 2016. A multi-statistical approach for estimating the total output of CO₂ from diffusive
547 soil degassing by the accumulation chamber method. *International Journal of*
548 *Greenhouse Gas Control* 47, 351-363.

549

550 Elskens, I., Tazieff, H., Tonani, F., 1964. A new method for volcanic gas analyses in
551 the field. *Bulletin Volcanologique* 27(1), 347-350.

552

553 Finizola, A., Ricci, T., Deiana, R., Cabusson, S.B., Rossi, M., Praticelli, N., Giocoli,
554 A., Romano, G., Delcher, E., Suski, B., Revil, A., Menny, P., Di Gangi, F., Letort, J.,
555 Peltier, A., Villasante-Marcos, V., Douillet, G., Avard, G., Lelli, M., 2010. Adventive
556 hydrothermal circulation on Stromboli volcano (Aeolian Islands, Italy) revealed by
557 geophysical and geochemical approaches: implications for general fluid flow models
558 on volcanoes. *Journal of Volcanology and Geothermal Research* 196(1-2), 111-119.

559

560 Finizola, A., Sortino, F., Lénat, J.F., Valenza, M., 2002. Fluid circulation at Stromboli
561 volcano (Aeolian Islands, Italy) from self-potential and CO₂ surveys. *Journal of*
562 *Volcanology and Geothermal Research* 116(1), 1-18.

563

564 Gaudin, D., Finizola, A., Delcher, E., Beauducel, F., Allemand, P., Delacourt, C.,
565 Brothelande, E., Peltier, A., Di Gangi, F., 2015. Influence of rainfalls on heat and steam
566 fluxes of fumarolic zones: Six months records along the Ty fault (Soufrière of
567 Guadeloupe, Lesser Antilles). *Journal of Volcanology and Geothermal Research* 302,
568 273-285.

569

570 Ghosh, J.K., Delampady, M., Samanta, T., 2006. *An Introduction to Bayesian Analysis:*
571 *Theory and Methods*. Springer-Verlag, New York.

572

573 Giammanco, S., Gurrieri, S., Valenza, M., 1997. Soil CO₂ degassing along tectonic
574 structures of Mount Etna (Sicily) : the Pernicana fault. *Applied Geochemistry* 12(4),
575 429-436.

576

577 Giammanco, S., Bellotti, F., Groppelli, G., Pinton, A., 2010. Statistical analysis reveals
578 spatial and temporal anomalies of soil CO₂ efflux on Mount Etna volcano (Italy).
579 *Journal of Volcanology and Geothermal Research* 194(1), 1-14.

580

581 Gresse, M., Vandemeulebrouck, J., Byrdina, S., Chiodini, G., Bruno, P. P., 2016.
582 Changes in CO₂ diffuse degassing induced by the passing of seismic waves. *Journal Of*
583 *Volcanology And Geothermal Research* 320, 12–18.

584

585 Gurrieri, S., Valenza, M., 1988. Gas transport in natural porous mediums : a method
586 for measuring CO₂ flows from the ground in volcanic and geothermal areas. *Rend. Soc.*
587 *Ital. Mineral. Petrol* 43, 1151-1158.

588

589 Hernández, P.A., Salazar, J.M., Shimoike, Y., Mori, T., Notsu, K., Pérez, N., 2001.
 590 Diffuse emission of CO₂ from Miyakejima volcano, Japan. *Chemical Geology* 177(1),
 591 175-185.
 592
 593 Hinkle, M.E., Dilbert, C.A., 1984. Gases and trace elements in soils at the North Silver
 594 Bell deposit, Pima County, Arizona. *Journal of Geochemical Exploration* 20(3), 323-
 595 336.
 596
 597 Irwin, W.P., Barnes, I., 1980. Tectonic relations of carbon dioxide discharges and
 598 earthquakes. *Journal of Geophysical Research : Solid Earth* 85(B6), 3115-3121.
 599
 600 Kucera, C., Kirkham, D.R., 1971. Soil respiration studies in tallgrass prairie in
 601 Missouri. *Ecology* 52(5), 912-915.
 602
 603 Liuzzo, M., Di Muro, A., Giudice, G., Michon, L., Ferrazzini, V., Gurrieri, S., 2015.
 604 New evidence of CO₂ soil degassing anomalies on Piton de la Fournaise volcano and
 605 the link with volcano tectonic structures. *Geochemistry, Geophysics, Geosystems*
 606 16(12), 4388-4404.
 607
 608 Liuzzo, M., Gurrieri, S., Giudice, G., Giuffrida, G., 2013. Ten years of soil CO₂
 609 continuous monitoring on Mt. Etna : Exploring the relationship between processes of
 610 soil degassing and volcanic activity. *Geochemistry, Geophysics, Geosystems* 14(8),
 611 2886-2899.
 612

613 Lovell, J.S., Hale, M., Webb, J.S., 1983. Soil air carbon dioxide and oxygen
614 measurements as a guide to concealed mineralization in semi-arid and arid regions.
615 *Journal of Geochemical Exploration* 19(1-3), 305-317.

616

617 Neri, M., Acocella, V., Behncke, B., 2004. The role of the Pernicana Fault System in
618 the spreading of Mt. Etna (Italy) during the 2002–2003 eruption. *Bulletin of*
619 *Volcanology* 66(5), 417-430.

620

621 Padrón, E., Melián, G., Marrero, R., Nolasco, D., Barrancos, J., Padilla, G., Hernández,
622 P.A., Pérez, N.M., 2008. Changes in the diffuse CO₂ emission and relation to seismic
623 activity in and around El Hierro, Canary Islands. In *Terrestrial Fluids, Earthquakes and*
624 *Volcanoes : The Hiroshi Wakita Volume III*, 95-114, Birkhäuser Basel.

625

626 Pearson, S.C.P., Connor, C.B., Sanford, W.E., 2008. Rapid response of a hydrologic
627 system to volcanic activity: Masaya volcano, Nicaragua. *Geology* 36(12), 951-954.

628

629 Revil, A., Finizola, A., Ricci, T., Delcher, E., Peltier, A., Barde-Cabusson, S., Avard,
630 G., Bailly, T., Bennati, L., Byrdina, S., Colonge, J., Di Gangi, F., Douillet, G., Lupi,
631 M., Letort, J., Tsang Hin Sun, E., 2011. Hydrogeology of Stromboli volcano, Aeolian
632 Islands (Italy) from the interpretation of resistivity tomograms, self-potential, soil
633 temperature and soil CO₂ concentration measurements. *Geophysical Journal*
634 *International* 186, 1078–1094, <https://doi.org/10.1111/j.1365-246X.2011.05112.x>.

635

636 Sandig, C., Sauer, U., Bräuer, K., Serfling, U., Schütze, C., 2014. Comparative study
637 of geophysical and soil–gas investigations at the Hartoušov (Czech Republic) natural
638 CO₂ degassing site. *Environmental earth sciences* 72(5), 1421-1434.

Sinclair, A.J., 1974. Selection of threshold values in geochemical data using probability graphs. *Journal of Geochemical Exploration* 3(2), 129-149.

Stephens, M.A., 1974. EDF Statistics for Goodness of Fit and Some Comparisons. *Journal of the American Statistical Association* 69, 730–737, doi:10.2307/2286009.

Stephens, M.A., 1976. Asymptotic Results for Goodness-of-Fit Statistics with Unknown Parameters. *Annals of Statistics* 4, 357-369.

Viveiros, F., Ferreira, T., Vieira, J.C., Silva, C., Gaspar, J.L., 2008. Environmental influences on soil CO₂ degassing at Furnas and Fogo volcanoes (São Miguel Island, Azores archipelago). *Journal of Volcanology and Geothermal Research* 177(4), 883-893.

Shinohara, H., 2005. A new technique to estimate volcanic gas composition: Plume measurements with a portable multi-sensor system. *J. Volcanol. Geotherm. Res.* 143, 319-333.

Zwillinger, D., Kokoska, S., 2000. *CRC Standard Probability and Statistics Tables and Formulae*. Chapman & Hall, New York.

Figures

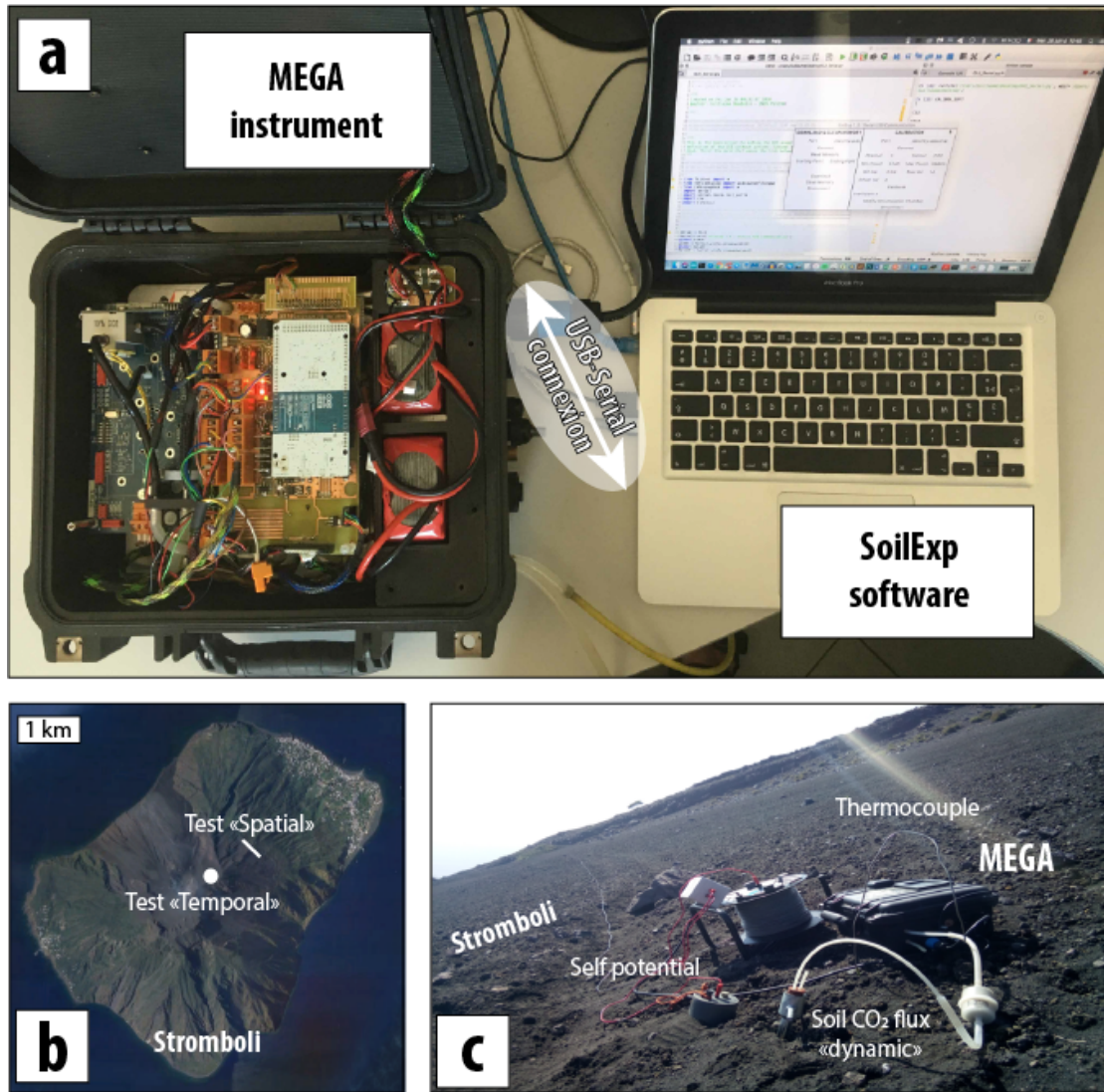


Fig. 1. (a) The MEGA instrument and the SoilExp software, in evidence the USB-Serial communication between the instrument and the software. (b) Tests of soil surveys at Stromboli (Sicily, Italy) (c) based on soil CO₂ flux, self-potential and ground temperature. These tests aim to illustrate the use of the SoilExp software in this study.

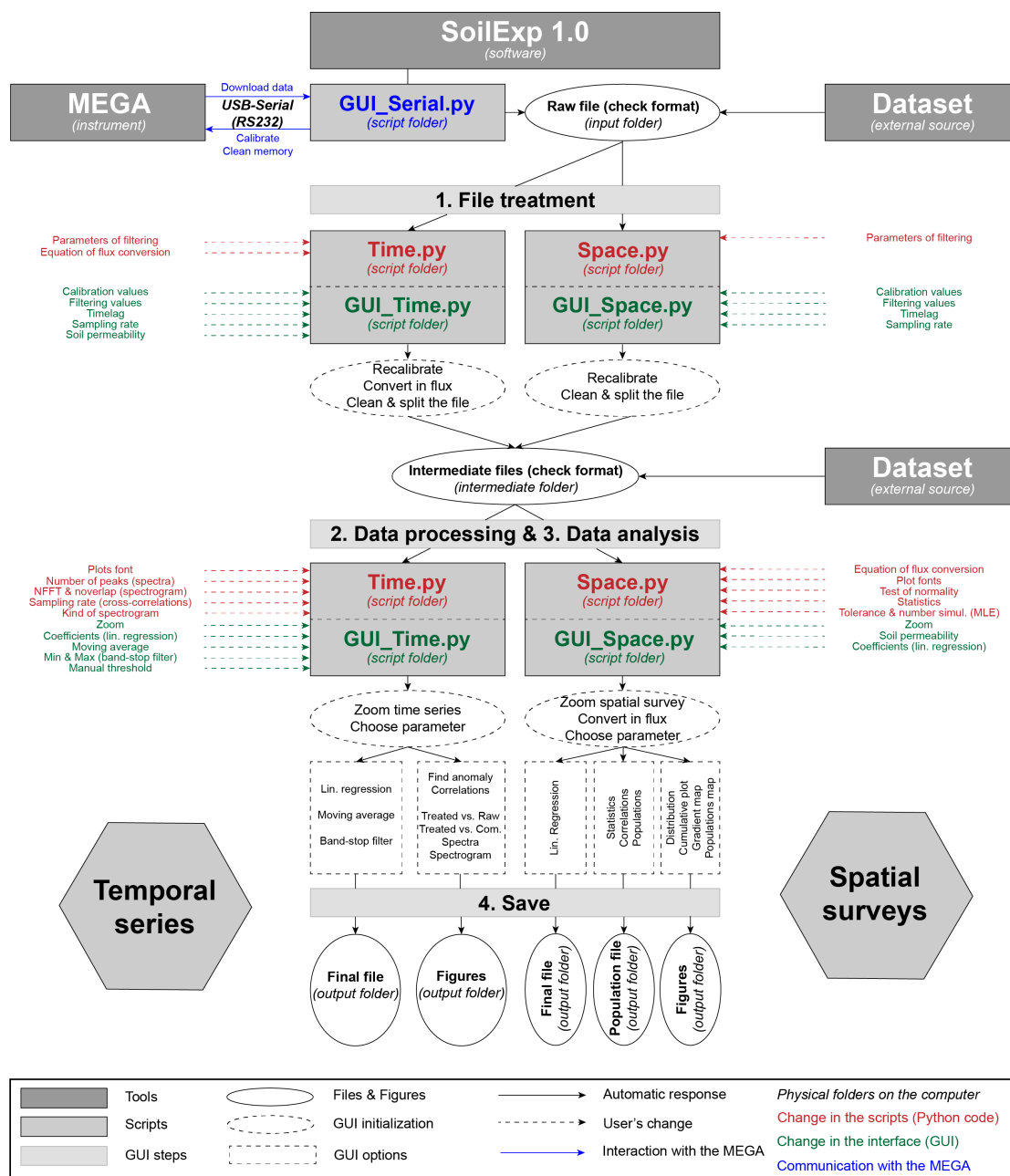
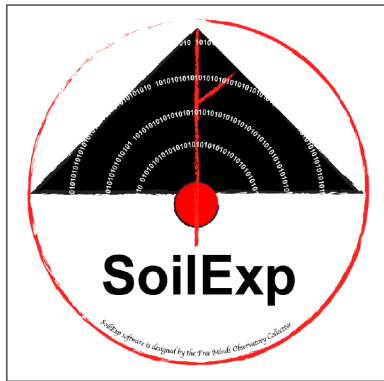


Fig. 2. General scheme of use of the SoilExp software applied either to dataset acquired with the MEGA instrument or though external sources.



SoilExp 1.0 : Serial USB Communication

DOWNLOAD & CLEAN MEMORY
Port
Connect
Read Memory
Starting Point Ending Point
Download
Clean Memory
Disconnect

CALIBRATION
Port
Connect
Channel Sensor
Min Count Max Count
Min Val Max Val
Offset Val
Calibrate
Coefficient K
Modify Accumulation Chamber
Disconnect

a

SoilExp 1.0 : Space

1. FILE TREATMENT
1a. Raw file
Load
1b. Linear Calibration
Parameter Slope Offset
Recalculate
1c. Treatment
TimeLag
Sampling Rate
Battery
Pump
HDOP
R-squared
Clean & Create

2. DATA PROCESSING
2a. Formatted file
Load & Init
2b. Subset
Start End
Zoom
Point Permeability ☒ All
Convert CO2
2c. Parameter
Choose the parameter to study
SP
Statistics
2d. Regression
Slope Param Offset
Correct

3. DATA ANALYSIS
3a. Correlations

	Slope	Offset	R2		Slope	Offset	R2
CO2_100	0.01	-122.1	0.18	V_FLUX	-0.16	207.48	0.02
P_atm	-0.00	1027.9	0.17	P_in	0.25	-559.0	0.05
CO2_10	0.03	-128.7	0.18	Rh	219.22	-741.6	0.09
T_atm	247.56	-4247.	0.21	T_in	-1.04	-53.94	0.01
SP	1.00	0.00	1.00	V_BAT	-22.90	189.72	0.00
SO2	147.28	8165.2	0.05	PUMP_FLUX	230.61	-369.4	0.09
H2S	394.12	7128.4	0.05	Thermocouple	-0.39	-131.7	0.04
PYR	-41557	59273.	0.06	CO2_FLUX	nan	nan	nan

3b. Statistics
Mean Median Min Max
Stdev Kurtosis Skewness N° Populations
Distribution Cumulative
3c. Maps
Google API API_KEY
Zoom (5-16)
Scatter Map (gradient) Scatter Map (populations)

4. SAVE
Save Spatial Survey
Save Populations

b

SoilExp 1.0 : Time

1. FILE TREATMENT
1a. Raw file
Load
1b. Linear Calibration
Parameter Slope Offset
Recalculate
1c. Treatment
TimeLag
Sampling Rate
Battery
Pump
HDOP
Soil Permeability ☐
Clean & Split

2. DATA PROCESSING
2a. Formatted file
Load
2b. Initialize
Time Serie
Zoom start / stop
Initialize
2c. Process
Regression
MovAverage time window
CutBand min / max
Comparison
Treated vs. Raw Treated vs. Comparative
Spectra Spectrogram
Correlations Find Anomaly
Threshold

3. DATA ANALYSIS

	Slope	Offset	R2	Delay	R2
CO2_100	0.83	196.74	0.74	0.00	0.74
P_atm	-15.52	15849.	0.05	323.00	0.19
CO2_10	1.00	0.00	1.00	0.00	1.00
T_atm	-72.34	2706.6	0.02	255.00	0.15
SP	-1.57	1435.1	0.00	60.00	0.14
SO2	-26.72	-0.71	0.00	422.00	0.22
H2S	-70.18	211.44	0.00	422.00	0.22
PYR	-14358	22025.	0.02	444.00	0.13
V_FLUX	nan	nan	nan	0.00	nan
P_in	-0.02	1536.9	0.00	665.00	0.15
Rh	6.75	1484.3	0.00	666.00	0.03
T_in	0.49	1478.8	0.00	409.00	0.15
V_BAT	-62.42	2302.6	0.00	668.00	0.04
PUMP_FLUX	6.69	1496.1	0.00	666.00	0.03
Thermocouple	nan	nan	0.00	0.00	0.00

4. SAVE
Save Time Serie

c

Fig. 3. Graphical User Interface (GUI) of the “Serial” (a), “Space” (b) and “Time” (c) option of the SoilExp software. The GUI is divided in 4 panels. Panel (1) is dedicated to format the raw file in intermediate formatted files after applying potential distinct calibrations and conversions, and cleaning the dataset. Panel (2) aimed to process the data obtained from the intermediate formatted files either from the previous step or formatted independently by the user (conversion, moving average, linear regression, cut band filter). Panel (3) shows the result of the datasets processing and analysis (correlations, cross-correlations, statistics, analysis of populations, distribution, maps). Panel (4) allows to save the dataset transformed with the above operations in final .csv file.

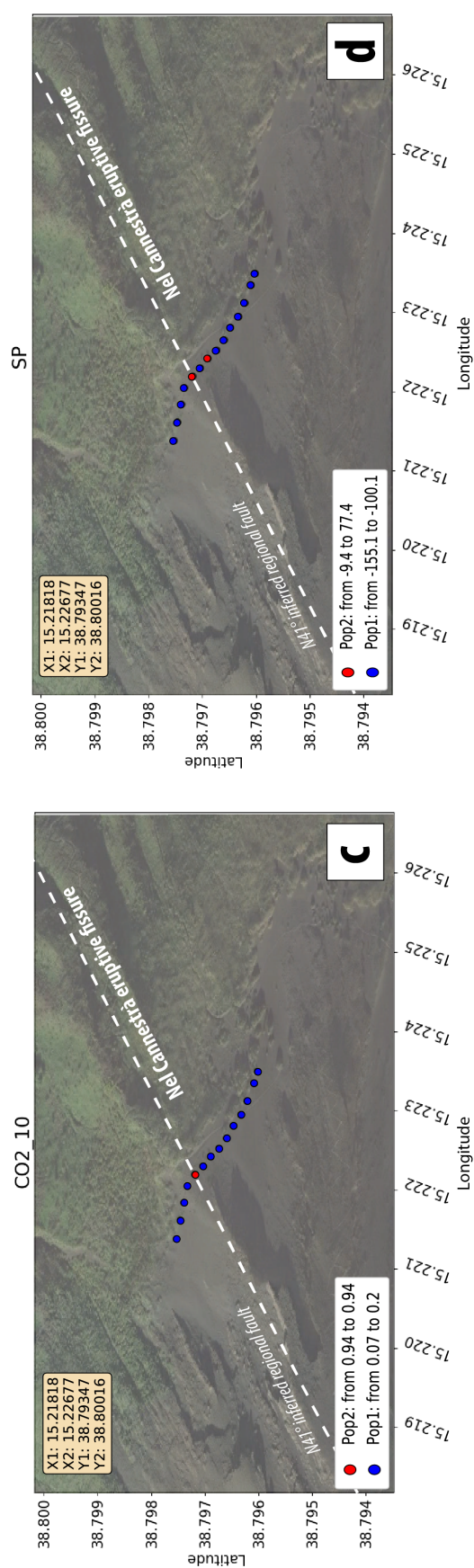
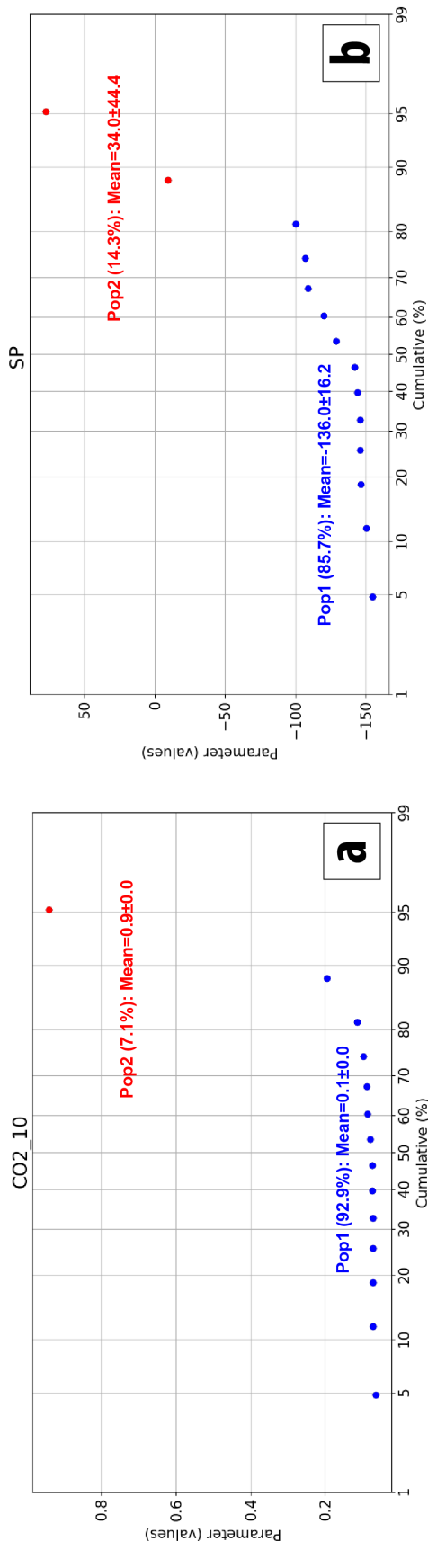


Fig. 4. Example of data analysis obtained by using the “Space” option at Stromboli (soil CO₂ flux and self-potential measurements along a transect with a 20 m-spacing; cf. Test “Spatial” on Fig. 1c, d). Probability plot of (a) soil CO₂ flux measurements obtained using a 0-10 %molar IR spectrometer (e.g. CO₂_10 by “dynamic” concentration; Gurrieri & Valenza, 1988; Camarda *et al.*, 2006) and (b) self-potential measurements carried out with a pair of non-polarizable Cu/CuSO₄ electrodes (e.g. SP; Finizola *et al.*, 2010). The identification of distinct populations is based on the maximum-likelihood numerical method (see text). Map highlighting the corresponding (c) soil CO₂ flux and (d) self-potential transect performed at Stromboli (cf. Fig. 1). The satellite map is obtained from Google Map. In case of absence of API key (<https://developers.google.com/maps/documentation/javascript/get-api-key>), the background will stay white. However, the (decimal) coordinates of the corners are reported in the upper left box in order to let the user free to download a map from distinct sources. In this example, the “Space” option allows to identify a soil CO₂ anomaly coupled with a positive SP anomaly that highlight an upward migration of hydrothermal fluids along the Nel Cannestrà eruptive fissure. This result is in accordance with previous study (Finizola *et al.*, 2002, 2010; Carapezza *et al.*, 2009).

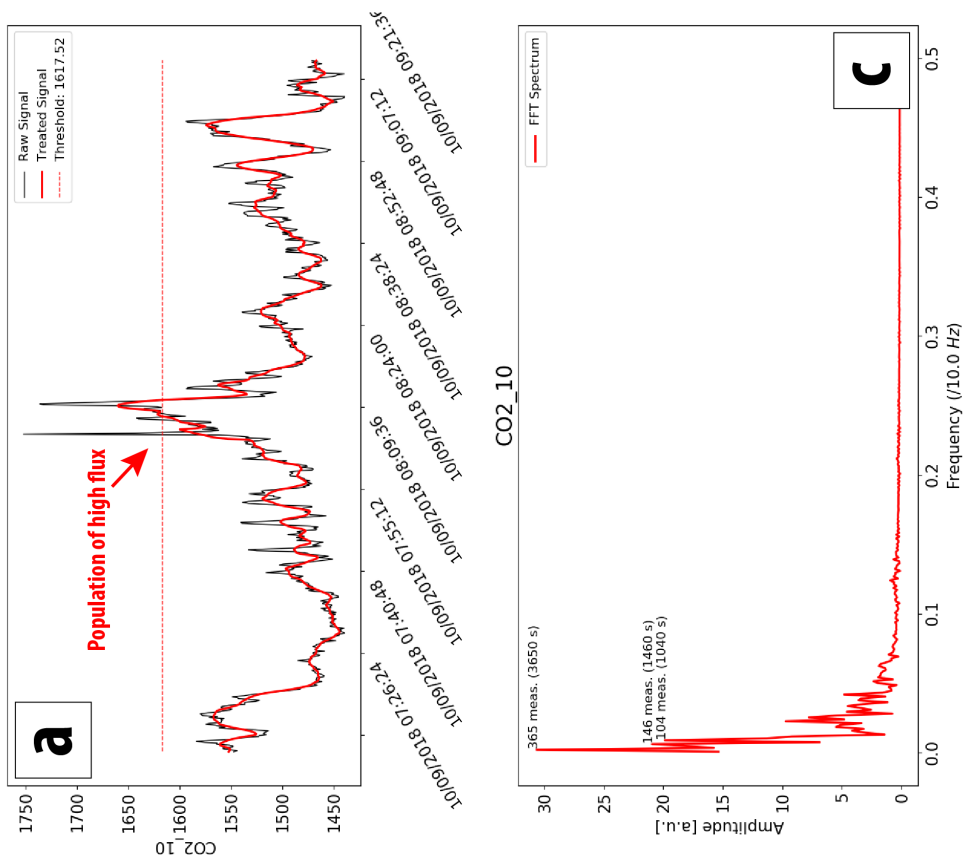


Fig. 5. Example of data analysis obtained by using the “Time” option at Stromboli (soil CO₂ flux measured during about 2 hours at 0.1 Hz at the same site; cf. Test “Temporal” on Fig. 1b). (a) Comparison between raw and treated data (after applying the moving average). The threshold analysis allows us to detect the highest population of values (often considered as “anomalous” values) during the acquisition. (b) Comparison between treated soil CO₂ flux (e.g. CO2_10) and self-potential (e.g. SP) time series. Here the detected soil CO₂ flux anomaly is synchronous with low self-potential records. (c) Fast Fourier Transform (FFT) spectrum of the treated soil CO₂ signal. The 3 greatest frequency peaks are labelled with the corresponding period that may be cut using the cut band filter. (d) Spectrogram of the treated soil CO₂ signal (linear detrend; magnitude mode; NFFT=256; noverlap=128). In this example, with about 1200 measurements, there are not enough data available to obtain a smoothed spectrogram considering a NFFT of 256.